CHEMISTRY OF MATERIALS

Article

pubs.acs.org/cm

Ultrathin Supercapacitor Electrode Based on Reduced Graphene Oxide Nanosheets Assembled with Photo-Cross-Linkable Polymer: Conversion of Electrochemical Kinetics in Ultrathin Films

Kiyoung Jo,[†,∥,⊥] Minsu Gu,[§,⊥] and Byeong-Su Kim*[,‡,§]

[†]Department of Physics, [‡]Department of Chemistry, School of Natural Science, and [§]Department of Energy Engineering, School of Energy and Chemical Engineering, Ulsan National Institute of Science and Technology (UNIST), Ulsan 689-798, Korea

[∥]Photo-Electronic Hybrids Research Center, Korea Institute of Science and Technology (KIST), Seoul 136-791, Korea

Supporting Information

ABSTRACT: An ultrathin supercapacitor electrode based on reduced graphene oxide (rGO) nanosheets is prepared using Layer-by-Layer (LbL) assembly. The rGO nanosheets functionalized with a conducting polymer, poly(3,4-ethylene dioxythiophene):poly(styrenesulfonate) (PEDOT:PSS), were assembled using a photo-cross-linkable diazoresin (DR). The unique photo-cross-linking property of the DR polymer enabled the conversion of the ionic bonds in the LbL-assembled film to covalent bonds upon UV irradiation, significantly enhancing the overall electrochemical activity of the resulting ultrathin supercapacitor electrode. By UV/vis and Fourier transform infrared (FT-IR) spectroscopy measurements, we proved that decomposition of the diazonium group from DR, followed by covalent bond formation, contributed to the enhanced integrity of the adjacent interfaces within the multilayers. In particular, electrochemical measurements suggested that a charge transfer process is facilitated after cross-linking, which resulted in a considerable increase in the volumetric capacitance. The hybrid thin film of the rGO supercapacitor exhibited a capacitance of 354 F/cm^3 at a scan rate of 20 mV/s and maintained a capacitance of 300 F/cm^3 even at a high scan rate of 200 mV/s, thus outperforming many other thin film supercapacitors.

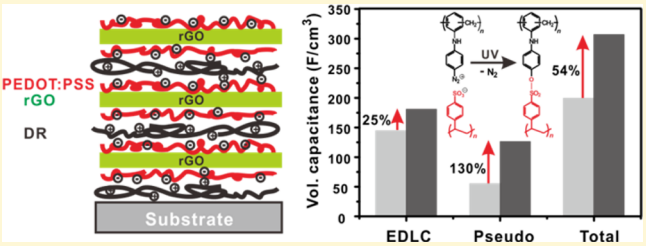

INTRODUCTION

Layer-by-Layer (LbL) assembly has been widely used as a simple yet versatile method of fabricating controlled nanostructures on a surface.[1,2] In this method, a substrate is sequentially dipped into positively and negatively charged colloidal suspensions, which enables the creation of highly tunable, functional thin films with nanometer-level control of the structure, composition, and properties. With new advances in LbL assembly, a wide variety of materials other than simple polyelectrolytes, including polymeric micelles, biomolecules, carbon nanotubes, and graphene, have been explored for use as active building blocks.[1,3−5] Incorporation of a broader range of nanomaterials using LbL assembly has expanded the potential applications of LbL structures in various fields ranging from energy and electrochemical devices to biological materials.[4,6,7] Typically, LbL assemblies rely on electrostatic interactions, which are stronger than many other types of intermolecular interactions used, such as hydrogen bonding,[8,9] charge-transfer interactions,[10] and coordination bonding.[11,12] Nevertheless, these interactions are weakened by high ionic strength, extreme pH, and strongly polar solvents, which consequently limit the applications of the assembled thin films in specific fields.

Alternatively, the stability of LbL multilayer thin films can be greatly enhanced by the conversion of electrostatic interactions into covalent interactions. Kotov and co-workers employed the covalent cross-linking strategy to impart intrinsic strength to a polymer−single-walled carbon nanotube (SWNT) composite.[13] They also found that the tensile strength of cross-linked composites was several times higher than that of a similar SWNT composite prepared by a simple mixing process. In this context, diazoresins (DRs), which are products of polycondensation of a diarylamine-4-diazonium salt or its derivatives with formaldehyde, are particularly attractive.[14] Integration of positively charged DRs into multilayer thin films with other anionic polyelectrolytes has been demonstrated to yield films with high stability due to the conversion of ionic linkages into covalent bonds upon UV treatment.[15]

Incorporation of active carbon nanomaterials such as graphene and carbon nanotubes into various hybrid materials is attracting significant interest because of their unique electrical, optical, and mechanical properties of such nanomaterials.[16] In particular, a thin film supercapacitor composed of active carbon materials such as reduced graphene oxide (rGO) offers an intriguing opportunity for capacitive behavior because of its high electrical conductivity, mechanical stability, and large surface area.[17−19] Furthermore, rGO can contribute to the

Received: August 25, 2015
Revised: November 9, 2015
Published: November 9, 2015

DOI: 10.1021/acs.chemmater.5b03296
Chem. Mater. 2015, 27, 7982−7989

enhancement of the electrochemical stability of pseudocapacitive materials, which generate electrochemical current through a direct redox reaction. Because pseudocapacitive materials are generally severely degraded with the number of pseudocapacitive cycles, rGO can provide a stable framework for such materials. Moreover, graphene itself shows capacitance because of the formation of an electric double layer, as it facilitates physical accumulation of charges on the solid−liquid interface because of its high electrical conductivity and large surface area.[18,20] Despite these favorable features, the use of graphene and related carbon materials in supercapacitors is still limited due to their low capacitance (typically in the range of 10−10^2 F g^{-1}), as the electric double-layer capacitance (EDLC) is typically much lower than that of pseudocapacitance resulting from the faradaic redox reaction.[21] Thus, hybrid materials that exhibit pseudocapacitance have been actively introduced to complement the performance of rGO. Much effort has been devoted to integrate rGO with other electrochemically active components such as metal oxides, metals, semiconductors, and nanoparticles, with the aim of exploiting both the EDLC and the pseudocapacitance.[22−26] For example, a hybrid electrode consisting of an electric double-layer capacitor of graphene nanosheets and a pseudocapacitor of the conducting polymer polyaniline exhibits a synergistic effect with excellent electrochemical performance for flexible thin film supercapacitors. In these hybrid structures, pseudocapacitance is the major contributor to the total capacitance, although to the best of our knowledge, there has been no precise and quantitative analysis regarding this issue in the context of multilayers with graphene.[27,28]

In this study, rGO nanosheets functionalized with a conducting polymer [poly(3,4-ethylene dioxythiophene):poly(styrenesulfonate) (PEDOT:PSS)] via noncovalent interactions (rGO-PEDOT:PSS) were integrated into a multilayer film with a photo-cross-linkable DR (Scheme 1). Because of the unique photo-cross-linking property of the DR polymer, the electrochemical activity of the resulting ultrathin supercapacitor electrode based on the rGO-PEDOT:PSS film was significantly enhanced. Furthermore, we investigated the transfer mechanisms upon photo-cross-linking with respect to the film thickness in ultrathin film-based capacitive behavior.

Scheme 1. Layer-by-Layer Assembly of Photo-Cross-Linkable DR and rGO-PEDOT:PSS

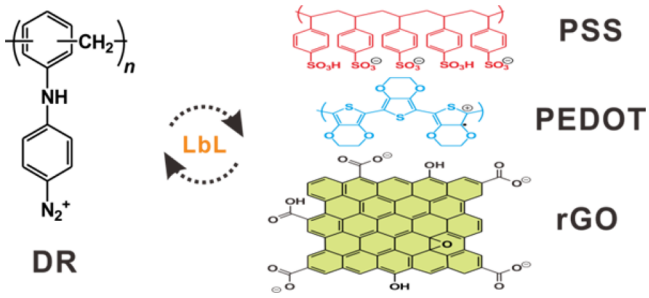

EXPERIMENTAL SECTION

Synthesis of Graphene Oxide (GO) Nanosheet. Graphite oxide was initially synthesized from graphite powder (Aldrich) by the modified Hummers method and immersed in deionized water.[29] Ultrasonication was subsequently performed to exfoliate the graphite oxide into a brown dispersion of graphene oxide (GO). The concentration of the dispersion was set to 0.50 mg/mL.

Synthesis of Diazoresin (DR). DR was synthesized according to the previous literature.[30] The average molecular weight (M_w) was measured to be 3000 g/mol using a polystyrene standard (see Figure S1). rGO-PEDOT:PSS was prepared as described in our previous study.[31] Briefly, GO was reduced with hydrazine in the presence of PEDOT:PSS (GO:PEDOT:PSS = 1:10, w/w), and the mixture was filtered to remove residual chemicals and free polymers. The resulting filter was redispersed in a known volume of water to give a stable suspension of rGO-PEDOT:PSS at a concentration of 0.50 mg/mL. All other reagents were obtained from Aldrich and used as received.

LbL Assembly. The LbL thin film was assembled on a silicon wafer, quartz slide, ZnSe slide, or indium tin oxide (ITO)-coated glass slide. All substrates were cleaned extensively before the LbL deposition. Each substrate was first treated with O_2 plasma for 2 min before use. The substrate was then dipped into a positively charged DR solution (0.50 mg/mL, pH 3.5) for 10 min, followed by three sequential rinsing steps with pH-adjusted water for 1 min each. Finally, the substrate was dipped into an rGO-PEDOT:PSS suspension (0.50 mg/mL, pH 4.5) for 10 min and subjected to the same rinsing steps as described above. This cycle provided a bilayer of DR and rGO-PEDOT:PSS; herein, the notation $(DR/rGO\text{-}PEDOT:PSS)_1$ will be used, where the numerical subscript indicates the number of bilayers. The dipping process was repeated until the desired number of bilayers was formed (n = 1−10). All fabrication processes were performed in the dark, and the prepared thin films were kept in the dark to prevent potential degradation of DR. Each sample was irradiated with UV light (at a wavelength of 365 nm) for 10 min, using a 100 W black incandescent lamp (365 nm Blak-Ray B-100AP High Intensity UV lamp, UVP) placed 20 cm from the sample.

Characterization. The absorbance of the samples was measured by UV/vis spectroscopy (Cary 5000, Varian). The thickness of the samples on the silicon substrates was obtained by ellipsometry (J. A. Woollam Co. Inc., EC-400 and M-2000 V). An LbL film on a ZnSe substrate was used to measure the IR spectra on a Fourier transform infrared (FT-IR) equipment (670-IR, Varian). Raman measurements (WITec alpha300R) were conducted with a 532 nm laser (1.0 mW). Surface morphology images were collected by a scanning electron microscope (SEM; Cold FE-SEM, Hitachi). All electrochemical measurements were performed with the potentiostat VSP from Bio-Logic Science Instruments, using a standard three-electrode cell. For electrochemical measurement, 1.0 M H_2SO_4 solution and Ag/AgCl electrode were utilized as electrolyte and reference electrode, respectively.

RESULTS AND DISCUSSION

Film Growth and Morphology Analysis. DR was first synthesized according to previously published protocols.[14,30] The rGO nanosheets were functionalized with the conventional conducting polymer PEDOT:PSS through noncovalent interactions as demonstrated in a previous report.[31] Briefly, a GO nanosheet was chemically reduced to rGO by hydrazine treatment in the presence of PEDOT:PSS (weight ratio of 1:10) to give a stable suspension of rGO-PEDOT:PSS at a concentration of 0.50 mg/mL. The ζ-potential of the rGO-PEDOT:PSS recorded −57 mV, suggesting successful formation of highly charged PSS layers surrounding the rGO nanosheets.

Elemental analysis showed that the rGO nanosheet content in the rGO/PEDOT:PSS nanocomposite was around 30%. Given these two stable suspensions, multilayer films of $(DR/rGO\text{-}PEDOT:PSS)_n$ (n = number of bilayers, BL) were assembled on a glass slide or silicon wafer by means of the electrostatic interactions between the positively charged DR ($DR\text{-}N_2^+$) and the negatively charged rGO-PEDOT:PSS, using LbL assembly.

Figure 1a shows the UV/vis absorbance spectra of the assembled $(DR/rGO\text{-}PEDOT:PSS)_n$ with different numbers of

DOI: 10.1021/acs.chemmater.5b03296
Chem. Mater. 2015, 27, 7982−7989

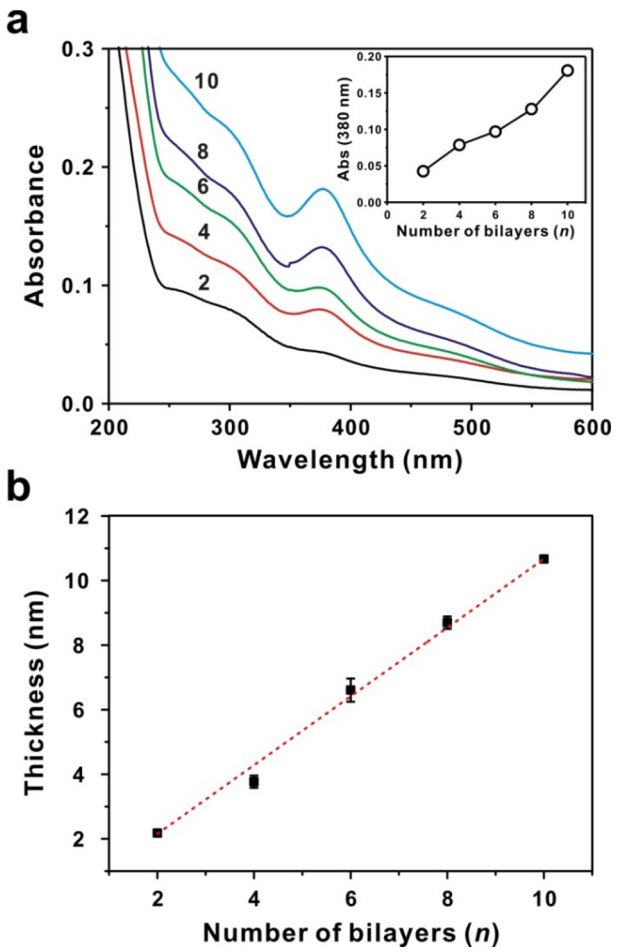

Figure 1. (a) Growth curve of $(DR/rGO\text{-}PEDOT:PSS)_n$ multilayer thin film with different numbers of bilayers. The number on each curve represents the number of bilayers. Inset shows the linear relationship between the absorbance of the film at 380 nm and the number of bilayers. (b) The thickness of $(DR/rGO\text{-}PEDOT:PSS)_n$ samples measured by ellipsometer.

bilayers. The absorbance of the multilayer film increased linearly with the number of bilayers. The absorbance at 380 nm was attributed to the $\pi-\pi^*$ transition of the diazonium group, whereas the absorbance at 270 nm corresponded to the conjugated backbone of the rGO nanosheets.[31−33] This result indicated that the deposition was uniform and that a similar amount of DR was deposited in each layer. Moreover, a constant mass of rGO nanosheets was assembled, as evidenced by the linear increase in the absorbance at 270 nm with the number of bilayers. Ellipsometry measurements further yielded an average thickness of about 10.7 nm for the 10 BL film, that is, a thickness of about 1.07 nm per bilayer considering the linear growth profile of the $(DR/rGO\text{-}PEDOT:PSS)_n$ multilayer film (Figure 1b). The control experiment performed on the multilayer film assembled without the rGO nanosheets, $(DR/PEDOT:PSS)_n$, also demonstrated a linear growth profile with an average bilayer thickness of 0.82 nm, which was slightly smaller than that of the $(DR/rGO\text{-}PEDOT:PSS)_n$ multilayer film.

Independent from the growth of the multilayers, Raman spectroscopy was examined to verify that all of the components were integrated within the multilayer (Figure S2). For example, the rGO nanosheet exhibited D and G peaks at 1300 and 1600 cm^{-1}, respectively, whereas Raman-inactive DR did not show any signals. PEDOT also displayed a characteristic Raman peak corresponding to the symmetric C=C vibration at ~1475 cm^{-1}, as previously reported.[34] The surface morphology of the multilayers was observed in the SEM (Figure S3). rGO multilayers were visible with a large coverage of more than several tens of micrometers with characteristic surface wrinkles on the graphene structure.

UV Cross-Linking. After monitoring the successful formation of LbL multilayers between the positively charged DRs and the negatively charged rGO-PEDOT:PSS on the basis of electrostatic interactions, we conducted UV cross-linking of DRs using a medium-pressure mercury lamp (100 W). Upon UV irradiation at 365 nm, the absorbance at 380 nm decreases dramatically with a concomitant increase in the absorbance at 290 nm (Figure 2). During UV irradiation, the diazonium

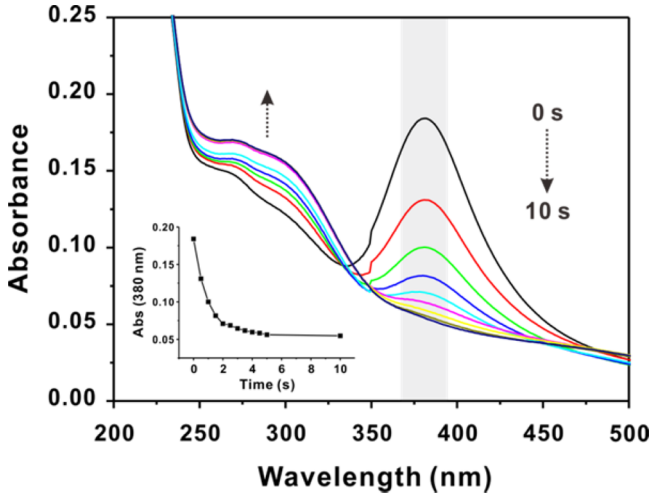

Figure 2. UV/vis spectra of $(DR/rGO\text{-}PEDOT:PSS)_{10}$ multilayer thin film under different UV irradiation times. Inset shows the relationship between the absorbance of the film at 380 nm and the UV irradiation time.

groups ($DR\text{-}N_2^+$) that are electrostatically assembled with sulfonate groups (SO_3^-) on the surface of rGO decompose to yield a phenyl cation (DR^+). This unstable phenyl cation reacts readily with adjacent sulfonate groups to produce aryl 4-styrenesulfonate groups, as depicted in Scheme 2. Because the

Scheme 2. Photochemical Cross-Linking Reaction between DR and rGO-PEDOT/PSS within the Multilayer Thin Film

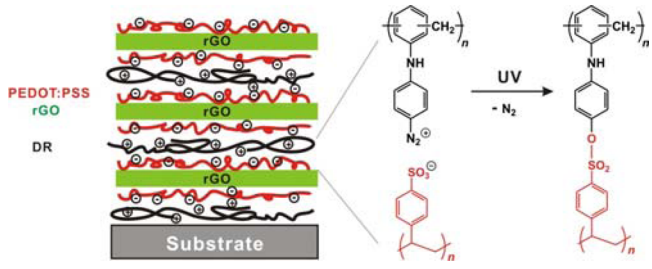

first step of diazonium decomposition is known to be the rate-determining step, the overall reaction is regarded as a unimolecular first-order reaction.[35] According to first-order kinetics, we calculated the rate constant for our reaction scheme to be 1.07 s^{-1}, which is significantly greater than the literature values. For example, Sun and co-workers reported a rate

DOI: 10.1021/acs.chemmater.5b03296
Chem. Mater. 2015, 27, 7982−7989

constant of 8.35×10^{-3} s^{-1} for their multilayer film consisting of DR and iron(III) tetrasulfophthalocyanine.[32] In our control experiment involving a plain $(DR/PEDOT:PSS)_{10}$ film without rGO, a rate constant of 0.71 s^{-1} was also obtained, which suggested that the enhanced kinetics of DR decomposition was attributable to the sulfonate groups on the flexible polymeric structure of PSS. However, the reaction between the carboxy acid group on the rGO might also participate in cross-linking as reported in literature.[36]

The formation of covalent linkages following the decomposition of the diazonium group ($DR\text{-}N_2^+$) was further verified by FT-IR measurements (Figure 3). The $(DR/rGO\text{-}PEDOT:PSS)_{20}$ multilayer thin film assembled on an IR-transparent ZnSe substrate was carefully monitored before and after UV irradiation. Two distinct peaks at 2170 and 2221 cm^{-1} were observed, which originated from the symmetric and asymmetric stretching vibration modes of the diazonium ion (N_2^+), respectively. After UV irradiation, however, these two peaks disappeared completely, indicating decomposition of the diazonium groups. Moreover, the strong absorbance at 1579 cm^{-1}, corresponding to phenyl groups in the diazonium moiety of DR, diminished markedly, with a subsequent peak shift to 1597 cm^{-1}. These results clearly demonstrated the successful decomposition of the diazonium group, followed by the formation of a covalent bond between DR and rGO-PEDOT:PSS. On the other hand, the symmetric stretching peak due to the aromatic sulfonate groups (SO_3^-) in the $(DR/rGO\text{-}PEDOT:PSS)_{20}$ film at 1180 cm^{-1} shifted only slightly to 1173 cm^{-1}.

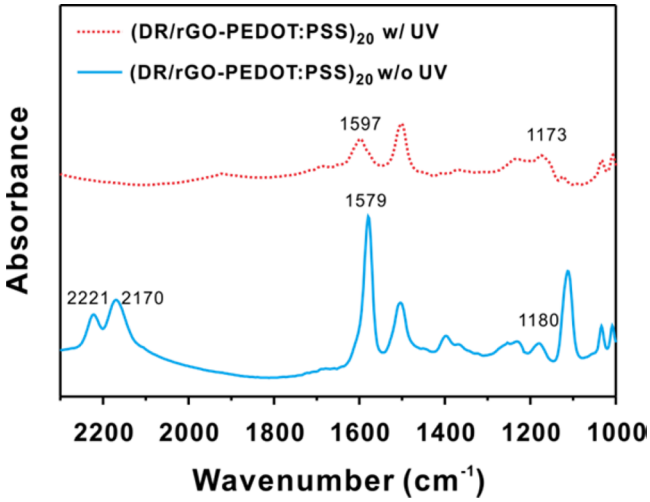

Figure 3. FT-IR spectra of $(DR/rGO\text{-}PEDOT:PSS)_{20}$ multilayer thin film assembled on a ZnSe substrate (solid line) before and (dotted line) after UV irradiation. Characteristic wavenumbers are labeled.

Electrochemical Analysis. The capacitive performance of the photo-cross-linked $(DR/rGO\text{-}PEDOT:PSS)_{10}$ thin film supercapacitor was evaluated using cyclic voltammetry (CV) at potential intervals from −0.2 to 1.0 V, using a Ag/AgCl electrode as the reference electrode and a platinum wire as the counter electrode. Volumetric capacitance (F/cm^3) and areal capacitance values (F/cm^2) were extracted using the following equation:

$$C_V = \frac{1}{\nu \Delta V A t} \oint i \, dV \quad (1)$$

where ν is the scan rate (V/s), ΔV is the potential range (V), A is the area (cm^2), and t is the thickness (cm) obtained from ellipsometry measurements. The electrochemical performance of the $(DR/PEDOT:PSS)_{10}$ control film was also investigated to understand the contribution of rGO to the capacitive behavior. The hybrid supercapacitor based on rGO nanosheets functionalized with the conducting polymer PEDOT:PSS exhibited broad redox peaks in the potential ranges investigated, indicating typical pseudocapacitive behavior (Figure 4a). Interestingly, UV irradiation resulted in a remarkable increase in the current density and the corresponding volumetric capacitance reaching 306 F/cm^3 by 54%, illustrating that photo-cross-linking between DR and PSS improved the capacitive performance (Figure 4b). On the other hand, the $(DR/PEDOT:PSS)_{10}$ film showed a modest decrease of 27% from 119 to 87.3 F/cm^3 in capacitance upon photo-cross-linking (Figure 4c). It is of note that the volumetric capacitance values were calculated from −0.2 to 0.8 V to exclude contribution of irreversible oxidation within 0.8−1.0 V to the nonfaradaic region. Taking these results together, we can account for the higher capacitance by the presence of the rigid rGO framework, which firmly protects the PEDOT:PSS structure during the redox reaction.

Furthermore, we hypothesized that rGO prevents side reactions, especially not directional cross-linking between DR and PEDOT. Because the photo-cross-linking reaction is very fast, as shown in Figure 3, such side reactions are inevitable. To prove this hypothesis, we separated the capacitance value into nonfaradaic and faradaic components, which are the EDLC and pseudocapacitance, respectively (Figure 4b,c and Figure S4). The $(DR/rGO\text{-}PEDOT:PSS)_{10}$ set displayed a 160% increase in pseudocapacitance, whereas $(DR/PEDOT:PSS)_{10}$ showed a 48% decrease in pseudocapacitance because of the damage to the PEDOT during the cross-linking process. On the other hand, PEDOT:PSS combined with rGO maintained the redox peak because of the alternative bonding of various functional groups in rGO with DR when the amount of PSS was insufficient. Note that the number of PSS groups is also important for photo-cross-linking, because a lack of PSS results in a similar degradation of the capacitance (Figure S5). When a low proportion of PEDOT:PSS was used to prepare the rGO-PEDOT:PSS, for example, a 1:1 weight ratio of rGO to PEDOT:PSS, the electrochemical activity was significantly degraded after UV exposure. Moreover, the EDLC increased slightly by 30%, indicating that the formation of covalent bonds between rGO and DR contributes to the enhancement of the EDLC. Because the backbone of PEDOT:PSS is tightly bound to rGO by $\pi-\pi$ interactions, degradation of the capacitance can be considerably prevented. As a result, due to the formation of covalent bonds after UV treatment, the specific capacitance reached 354 F/cm^3 at a scan rate of 20 mV/s, and a capacitance of 300 F/cm^3 was observed even at a higher scan rate of 200 mV/s. On the other hand, the film without UV treatment showed severely degraded capacitance as the scan rate was increased (Figure S6). The capacitance values are comparable to previously determined values, indicating that the thin film prepared in the current study can be used in practical supercapacitors.[15,18,37−39]

To further elucidate the transfer mechanisms in ultrathin film-based capacitive behavior, which is governed by two types of rate-determining steps, a diffusion limited mass transfer process and a surface-confined charge transfer process,[40] CV curves of the $(DR/rGO\text{-}PEDOT:PSS)_n$ (n = 2−10) films were

DOI: 10.1021/acs.chemmater.5b03296
Chem. Mater. 2015, 27, 7982−7989

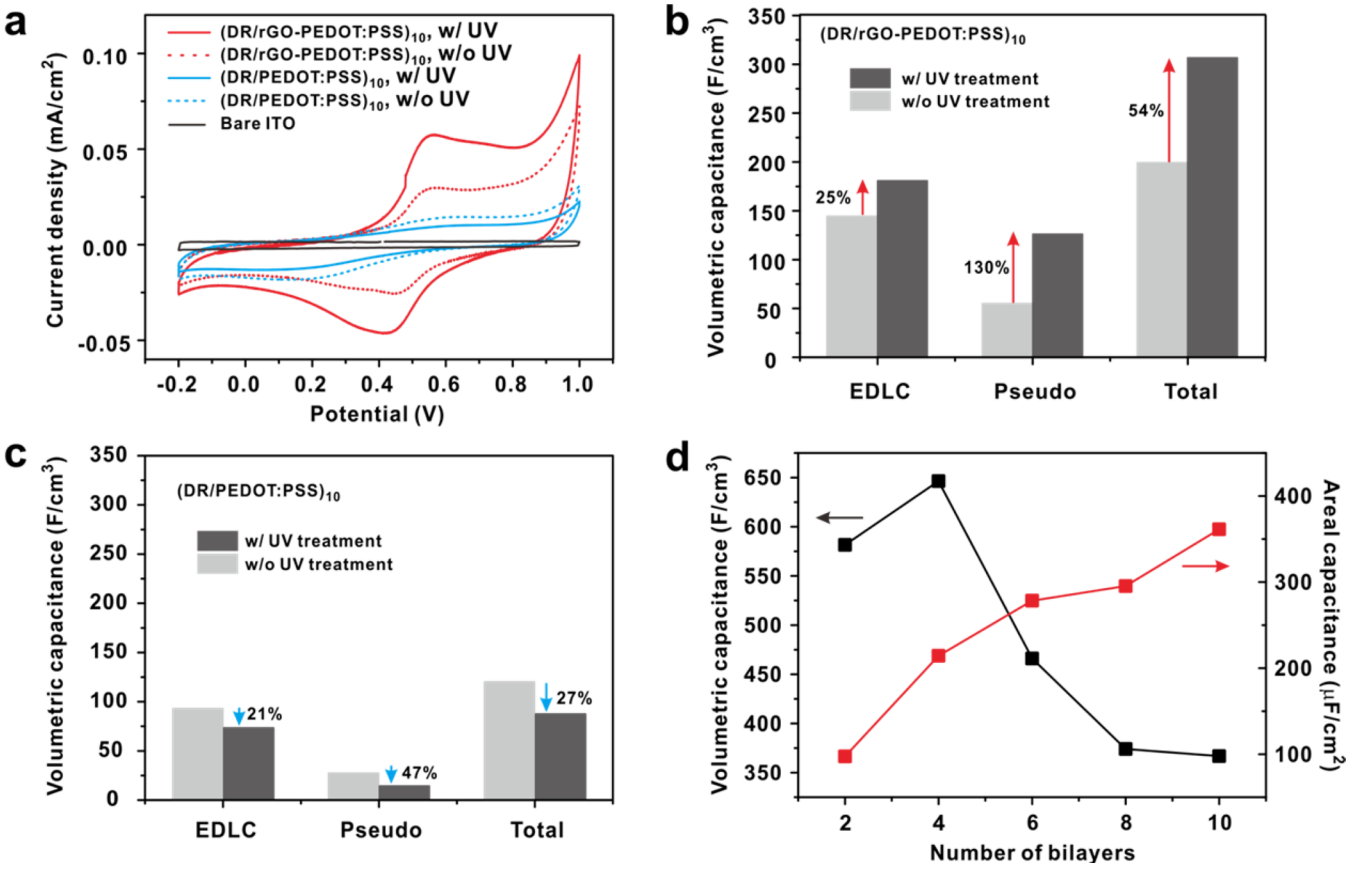

Figure 4. (a) Representative cyclic voltammogram curves of $(DR/rGO\text{-}PEDOT:PSS)_{10}$ and $(DR/PEDOT:PSS)_{10}$ at 100 mV/s before (dotted line) and after (solid line) UV treatment. Bare ITO-glass substrate was included for comparison. (b,c) EDLC and pseudocapacitance portions of $(DR/rGO\text{-}PEDOT:PSS)_{10}$ and $(DR/PEDOT:PSS)_{10}$, respectively. To eliminate irreversible oxidation region, the capacitance values were calculated in the range from −0.2 to 0.8 V. (d) Volumetric and areal capacitance of each layer after UV treatment.

collected, and volumetric capacitances were extracted (Figure 4d and Figure S7a). The 10 BL sample was found to have the maximum areal capacitance, whereas the 4 BL sample had the highest volumetric capacitance. This variance may be due, in part, to the increase in thickness. Under this nanoscale thickness where the mass transfer is negligible, a surface-confined system is established and charge transfer becomes the main rate-determining step, called by charge-transfer-limited system. However, as the number of bilayers increases, diffusion of the electrolyte provides another source of resistance. As a result, the capacitive behavior of a thick film is governed mainly by diffusion-limited mass transfer processes. As indicated in Figure 4d, the diffusion-limited resistance is negligible in thin films (up to 4 BL), whereas it dramatically diminishes the volumetric capacitance of thicker (6−10 BL) films. On the basis of these results, it can be inferred that the resistance from a mass transfer process significantly degrades the electrochemical activity as the thickness increases. Clearly, it is interesting to observe that the trade-off between the two processes is optimally balanced in the 4 BL film.

Furthermore, because the bonding characteristics and charge balance change after UV treatment, the origin of the capacitance variation after UV treatment can be elucidated if quantitative comparison is possible. For that purpose, we introduced a simple relationship for a quantitative analysis of the rate-determining step in the samples. First, the diffusion-limited process is described by the Randles−Sevcik equation, which expresses the peak current density in a reversible redox reaction as follows:

$$i = (2.69 \times 10^5) n^{3/2} A D_O^{1/2} C_O^* \nu^{1/2} \quad (2)$$

where n is the number of electrons transferred during the redox reaction, A is the area (cm^2), D_O is the diffusion coefficient (cm^2/s), C_O^* is the bulk concentration of redox components (mol/cm^3), and ν is the scan rate (V/s). According to this relationship, the peak current density is proportional to $\nu^{1/2}$, and the diffusion process mainly limits the capacitive currents ($i \propto \nu^{1/2}$).[41] In addition, as the multilayer film is extremely thin, current from the redox reaction is not influenced by diffusion; therefore, the diffusion coefficient is insignificant in the system. For this reason, it can be assumed that only adsorbed electroactive components react on the surface of the film; such a system is referred to as a surface-confined system. In a reversible and extremely thin system, the peak current density is given as follows:

$$i = \frac{n^2 F^2 \nu A \Gamma_O^*}{4RT} \quad (3)$$

where F is the Faraday constant (C/mol), Γ_O^* is the amount of redox components (mol/cm^2), R is the ideal gas constant (J/K·mol), and T is the temperature (K). This relationship reveals that the peak current density is directly proportional to the scan rate when the film is sufficiently thin ($i \propto \nu$).[42,43] To evaluate the rate-determining process for each set, plots of the peak

DOI: 10.1021/acs.chemmater.5b03296
Chem. Mater. 2015, 27, 7982−7989

current density versus the scan rate were obtained (Figure 5 and Figure S8). The p value collected from the fitting of the

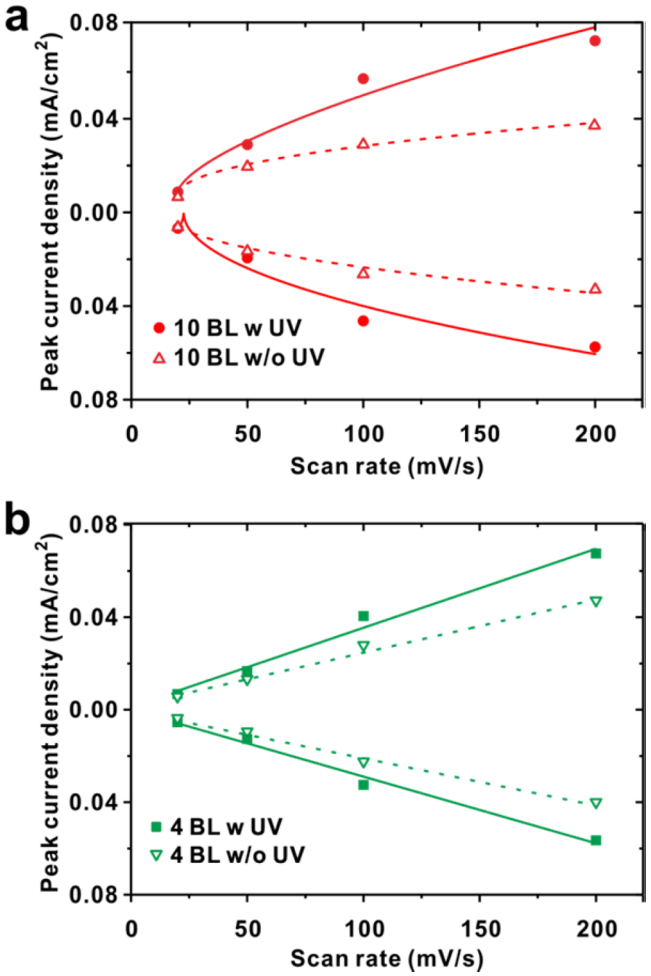

Figure 5. Current density versus scan rate plots for $(DR/rGO\text{-}PEDOT:PSS)_n$ at (a) n = 10 BL and (b) n = 4 BL before (dotted line) and after (solid line) UV treatment.

data of the $(DR/rGO\text{-}PEDOT:PSS)_{10}$ film was significantly altered after UV treatment (see Table S1). The film before UV treatment had a p value of 0.474, which is fairly close to the ideal value of 0.5; capacitive current was conducted mainly through a typical mass-transfer-limited process. Interestingly, after UV treatment, the film yielded an increased p value of 0.656 (Figure 5a). Although the main transfer limit still originates from mass transfer, this result suggests that the formation of covalent bonds facilitates the charge transfer process. Considering the increase in the volumetric capacitance, especially pseudocapacitance and p value after UV treatment, charge transfer facilitation due to cross-linking in the $(DR/rGO\text{-}PEDOT:PSS)_{10}$ film clearly results in a significant increase in the capacitance value. Further, the capacitance value of the 4 BL film showed a p value of ca. 1.0, so the charge transfer process predominantly determines the electrochemical activity (Figure 5b). This trend is in good agreement with Figure 4d in terms of the transition of the electrochemical-current-limiting mechanism from charge transfer to mass transfer. Interestingly, the trade-off thickness for charge transfer to mass transfer as the dominant process, ~4 nm, is much lower than that previously reported; for example, a 195 nm-thick film composed of vanadium contained small molecules.[42] This may be due to the unique characteristic of the layered architecture by two-dimensional building block of GO sheets. The CV curves for various numbers of bilayers also agree well with the above trend. The anodic/cathodic peak-to-peak separation (ΔE_p) gradually increases from 0.21 to 0.28 with increasing number of bilayers (Figure S7b). Because a higher overpotential is necessary for a large mass transfer resistance, mass transfer becomes more critical than charge transfer as the number of layers increases. Similarly, impedance data also reveal the charge transfer resistance reduces as the number of layers increases (Table S2 and Figure S9). Comparing the R_{ct} value of each set, UV treatment reduces charge transfer resistance in both 4 and 10 BL sets. In that regards, charge transfer is facilitated through photo-cross-linking. Charge/discharge curves from galvanostat accord with a previous description on the influence of UV treatment enhancing the performance of electrode (Figure S10). Although there was no considerable difference in the internal resistance values upon photo-cross-linking, the difference became significant with increase in the number of layers. From this observation, we argue that mass transfer resistance takes a significant role in determining overall internal resistance by interfering ionic diffusion in charging/discharging process as the number of layers increases.

CONCLUSION

An ultrathin supercapacitor electrode was fabricated by solution-processable LbL assembly of rGO nanosheets with a photo-cross-linkable polymer. UV treatment triggered cross-linking of DR with PEDOT:PSS, causing pure electrostatic interactions to convert to covalent bonds. The $(DR/rGO\text{-}PEDOT:PSS)_{10}$ film exhibited a large volumetric capacitance value of 354 F/cm^3, which is attributed to significant enhancement of the pseudocapacitance from PEDOT:PSS. Furthermore, electrochemical measurements suggested that photo-cross-linking between DR and PEDOT:PSS facilitates charge transfer, yielding a fairly large capacitance value of 300 F/cm^3 even at a high scan rate of 200 mV/s. Through solution-processable LbL assembly, various colloidal building blocks can be incorporated via electrostatic interactions, so future applications to thin film supercapacitors can be developed. Furthermore, we anticipate that the study will offer a model system to elucidate the electrochemical pathways governing the development of high-performance thin film supercapacitors.

ASSOCIATED CONTENT

Supporting Information

The Supporting Information is available free of charge on the ACS Publications website at DOI: 10.1021/acs.chemmater.5b03296.

Additional polymer and multilayer electrode characterization data; and GPC, Raman, SEM, and electrochemical analysis (PDF)

AUTHOR INFORMATION

Corresponding Author

*E-mail: bskim19@unist.ac.kr.

Author Contributions

⊥K.J. and M.G. contributed equally.

Notes

The authors declare no competing financial interest.

DOI: 10.1021/acs.chemmater.5b03296
Chem. Mater. 2015, 27, 7982−7989

■ ACKNOWLEDGMENTS

This work was supported by the National Research Foundation of Korea (NRF) grant (2014R1A2A1A11052829, 2015R1A2A2A04003160). K.J. and M.G. acknowledge the financial support from the Global Ph.D. Fellowship funded by the National Research Foundation of Korea (NRF-2013H1A2A1033123, NRF-2013H1A2A1033278).

■ REFERENCES

(1) Decher, G. Fuzzy Nanoassemblies: Toward Layered Polymeric Multicomposites. *Science* **1997**, *277*, 1232−1237.
(2) Hammond, P. T. Form and Function in Multilayer Assembly: New Applications at the Nanoscale. *Adv. Mater.* **2004**, *16*, 1271−1293.
(3) Kim, B.-S.; Smith, R. C.; Poon, Z.; Hammond, P. T. Mad (Multiagent Delivery) Nanolayer: Delivering Multiple Therapeutics from Hierarchically Assembled Surface Coatings. *Langmuir* **2009**, *25*, 14086−14092.
(4) Lee, S. W.; Kim, B. S.; Chen, S.; Shao-Horn, Y.; Hammond, P. T. Layer-by-Layer Assembly of All Carbon Nanotube Ultrathin Films for Electrochemical Applications. *J. Am. Chem. Soc.* **2009**, *131*, 671−679.
(5) Hong, T.-K.; Lee, D. W.; Choi, H. J.; Shin, H. S.; Kim, B.-S. Transparent, Flexible Conducting Hybrid Multi Layer Thin Films of Multiwalled Carbon Nanotubes with Graphene Nanosheets. *ACS Nano* **2010**, *4*, 3861−3868.
(6) DeMuth, P. C.; Moon, J. J.; Suh, H.; Hammond, P. T.; Irvine, D. J. Releasable Layer-by-Layer Assembly of Stabilized Lipid Nanocapsules on Microneedles for Enhanced Transcutaneous Vaccine Delivery. *ACS Nano* **2012**, *6*, 8041−8051.
(7) Tang, Z. Y.; Wang, Y.; Podsiadlo, P.; Kotov, N. A. Biomedical Applications of Layer-by-Layer Assembly: From Biomimetics to Tissue Engineering. *Adv. Mater.* **2006**, *18*, 3203−3224.
(8) Lee, H.; Mensire, R.; Cohen, R. E.; Rubner, M. F. Strategies for Hydrogen Bonding Based Layer-by-Layer Assembly of Poly(Vinyl Alcohol) with Weak Polyacids. *Macromolecules* **2012**, *45*, 347−355.
(9) Wang, L. Y.; Wang, Z. Q.; Zhang, X.; Shen, J. C.; Chi, L. F.; Fuchs, H. A New Approach for the Fabrication of an Alternating Multilayer Film of Poly(4-Vinylpyridine) and Poly(Acrylic Acid) Based on Hydrogen Bonding. *Macromol. Rapid Commun.* **1997**, *18*, 509−514.
(10) Shimazaki, Y.; Ito, S.; Tsutsumi, N. Adsorption-Induced Second Harmonic Generation from the Layer-by-Layer Deposited Ultrathin Film Based on the Charge-Transfer Interaction. *Langmuir* **2000**, *16*, 9478−9482.
(11) Xiong, H.; Cheng, M.; Zhou, Z.; Zhang, X.; Shen, J. A New Approach to the Fabrication of a Self-Organizing Film of Heterostructured Polymer/Cu_2S Nanoparticles. *Adv. Mater.* **1998**, *10*, 529−532.
(12) Schutte, M.; Kurth, D. G.; Linford, M. R.; Colfen, H.; Mohwald, H. Metallosupramolecular Thin Polyelectrolyte Films. *Angew. Chem., Int. Ed.* **1998**, *37*, 2891−2893.
(13) Mamedov, A. A.; Kotov, N. A.; Prato, M.; Guldi, D. M.; Wicksted, J. P.; Hirsch, A. Molecular Design of Strong Single-Wall Carbon Nanotube/Polyelectrolyte Multilayer Composites. *Nat. Mater.* **2002**, *1*, 190−194.
(14) Cao, W. X.; Zhao, C.; Cao, J. W. Synthesis and Characterization of 3-Methoxydiphenylamine-4-Diazonium Salt and Its Diazoresin. *J. Appl. Polym. Sci.* **1998**, *69*, 1975−1982.
(15) Xiong, Z.; Gu, T.; Wang, X. Self-Assembled Multi Layer Films of Sulfonated Graphene and Polystyrene-Based Diazonium Salt as Photo-Cross-Linkable Supercapacitor Electrodes. *Langmuir* **2014**, *30*, 522−532.
(16) Lee, T.; Min, S. H.; Gu, M.; Jung, Y. K.; Lee, W.; Lee, J. U.; Seong, D. G.; Kim, B.-S. Layer-by-Layer Assembly for Graphene-Based Multi Layer Nanocomposites: Synthesis and Applications. *Chem. Mater.* **2015**, *27*, 3785−3796.
(17) Hong, J.; Han, J. Y.; Yoon, H.; Joo, P.; Lee, T.; Seo, E.; Char, K.; Kim, B.-S. Carbon-Based Layer-by-Layer Nanostructures: From Films to Hollow Capsules. *Nanoscale* **2011**, *3*, 4515−4531.
(18) Zhang, L. L.; Zhou, R.; Zhao, X. S. Graphene-Based Materials as Supercapacitor Electrodes. *J. Mater. Chem.* **2010**, *20*, 5983−5992.
(19) Park, S.; Ruoff, R. S. Chemical Methods for the Production of Graphenes. *Nat. Nanotechnol.* **2009**, *4*, 217−224.
(20) Yoo, J. J.; Balakrishnan, K.; Huang, J. S.; Meunier, V.; Sumpter, B. G.; Srivastava, A.; Conway, M.; Reddy, A. L. M.; Yu, J.; Vajtai, R.; Ajayan, P. M. Ultrathin Planar Graphene Supercapacitors. *Nano Lett.* **2011**, *11*, 1423−1427.
(21) Simon, P.; Gogotsi, Y. Materials for Electrochemical Capacitors. *Nat. Mater.* **2008**, *7*, 845−854.
(22) Wu, Z. S.; Wang, D. W.; Ren, W.; Zhao, J.; Zhou, G.; Li, F.; Cheng, H. M. Anchoring Hydrous RuO_2 on Graphene Sheets for High-Performance Electrochemical Capacitors. *Adv. Funct. Mater.* **2010**, *20*, 3595−3602.
(23) Guo, S.; Dong, S.; Wang, E. Three-Dimensional Pt-on-Pd Bimetallic Nanodendrites Supported on Graphene Nanosheet: Facile Synthesis and Used as an Advanced Nanoelectrocatalyst for Methanol Oxidation. *ACS Nano* **2010**, *4*, 547−555.
(24) Bai, H.; Li, C.; Shi, G. Q. Functional Composite Materials Based on Chemically Converted Graphene. *Adv. Mater.* **2011**, *23*, 1089−1115.
(25) Kou, R.; Shao, Y.; Mei, D.; Nie, Z.; Wang, D.; Wang, C.; Viswanathan, V. V.; Park, S.; Aksay, I. A.; Lin, Y.; Wang, Y.; Liu, J. Stabilization of Electrocatalytic Metal Nanoparticles at Metal-Metal Oxide-Graphene Triple Junction Points. *J. Am. Chem. Soc.* **2011**, *133*, 2541−2547.
(26) Qu, Q.; Yang, S.; Feng, X. 2d Sandwich-Like Sheets of Iron Oxide Grown on Graphene as High Energy Anode Material for Supercapacitors. *Adv. Mater.* **2011**, *23*, 5574−5580.
(27) Dong, X.; Cao, Y.; Wang, J.; Chan-Park, M. B.; Wang, L.; Huang, W.; Chen, P. Hybrid Structure of Zinc Oxide Nanorods and Three Dimensional Graphene Foam for Supercapacitor and Electrochemical Sensor Applications. *RSC Adv.* **2012**, *2*, 4364−4369.
(28) Yan, J.; Fan, Z. J.; Wei, T.; Qian, W. Z.; Zhang, M. L.; Wei, F. Fast and Reversible Surface Redox Reaction of Graphene-MnO_2 Composites as Supercapacitor Electrodes. *Carbon* **2010**, *48*, 3825−3833.
(29) Hummers, W. S.; Offeman, R. E. Preparation of Graphitic Oxide. *J. Am. Chem. Soc.* **1958**, *80*, 1339−1339.
(30) Cao, W. X.; Ye, S. J.; Cao, S. G.; Zhao, C. Novel Polyelectrolyte Complexes Based on Diazo-Resins. *Macromol. Rapid Commun.* **1997**, *18*, 983−989.
(31) Jo, K.; Lee, T.; Choi, H. J.; Park, J. H.; Lee, D. J.; Lee, D. W.; Kim, B.-S. Stable Aqueous Dispersion of Reduced Graphene Nanosheets via Non-Covalent Functionalization with Conducting Polymers and Application in Transparent Electrodes. *Langmuir* **2011**, *27*, 2014−2018.
(32) Zhao, S.; Li, X. F.; Yang, M.; Sun, C. Q. Fabrication and Characterization of Covalently Attached Multilayer Films Containing Iron Phthalocyanine and Diazo-Resins. *J. Mater. Chem.* **2004**, *14*, 840−844.
(33) Qin, S. H.; Qin, D. Q.; Ford, W. T.; Zhang, Y. J.; Kotov, N. A. Covalent Cross-Linked Polymer/Single-Wall Carbon Nanotube Multilayer Films. *Chem. Mater.* **2005**, *17*, 2131−2135.
(34) Sakamoto, S.; Okumura, M.; Zhao, Z. G.; Furukawa, Y. Raman Spectral Changes of PEDOT-PSS in Polymer Light-Emitting Diodes Upon Operation. *Chem. Phys. Lett.* **2005**, *412*, 395−398.
(35) Sun, J. Q.; Wang, Z. Q.; Wu, L. X.; Zhang, X.; Shen, J. C.; Gao, S.; Chi, L. F.; Fuchs, H. Investigation of the Covalently Attached Multilayer Architecture Based on Diazo-Resins and Poly(4-Styrene Sulfonate). *Macromol. Chem. Phys.* **2001**, *202*, 967−973.
(36) Sun, J.; Wu, T.; Liu, F.; Wang, Z.; Zhang, X.; Shen, J. Covalently Attached Multilayer Assemblies by Sequential Adsorption of Polycationic Diazo-Resins and Polyanionic Poly(Acrylic Acid). *Langmuir* **2000**, *16*, 4620−4624.
(37) Tao, Y.; Xie, X.; Lv, W.; Tang, D.-M.; Kong, D.; Huang, Z.; Nishihara, H.; Ishii, T.; Li, B.; Golberg, D.; Kang, F.; Kyotani, T.; Yang, Q.-H. Towards Ultrahigh Volumetric Capacitance: Graphene Derived

DOI: 10.1021/acs.chemmater.5b03296
Chem. Mater. 2015, 27, 7982−7989

Highly Dense but Porous Carbons for Supercapacitors. *Sci. Rep.* **2013**, *3*, 2975−2982.
(38) Centeno, T. A.; Stoeckli, F. The Volumetric Capacitance of Microporous Carbons in Organic Electrolyte. *Electrochem. Commun.* **2012**, *16*, 34−36.
(39) Murali, S.; Quarles, N.; Zhang, L. L.; Potts, J. R.; Tan, Z.; Lu, Y.; Zhu, Y.; Ruoff, R. S. Volumetric Capacitance of Compressed Activated Microwave-Expanded Graphite Oxide (a-Mego) Electrodes. *Nano Energy* **2013**, *2*, 764−768.
(40) Bard, A. J.; Faulkner, L. R. *Electrochemical Methods: Fundamentals and Applications*, 2nd ed.; John Wiley & Sons: New York, 2000.
(41) Choi, Y.; Gu, M.; Park, J.; Song, H.-K.; Kim, B.-S. Graphene Multilayer Supported Gold Nanoparticles for Efficient Electrocatalysts toward Methanol Oxidation. *Adv. Energy Mater.* **2012**, *2*, 1510−1518.
(42) Fernandes, D. M.; Teixeira, A.; Freire, C. Multielectrocatalysis by Layer-by-Layer Films Based on Pararosaniline and Vanadium-Substituted Phosphomolybdate. *Langmuir* **2015**, *31*, 1855−1865.
(43) Fernandes, D. M.; Freire, C. Hybrid Photochromic Multilayer Films Based on Chitosan and Europium Phosphomolybdate. *J. Appl. Electrochem.* **2014**, *44*, 655−665.

DOI: 10.1021/acs.chemmater.5b03296
Chem. Mater. 2015, 27, 7982−7989